J. Fluid Mech. (2008), *vol.* 609, *pp.* 111–137. © 2008 Cambridge University Press
doi:10.1017/S0022112008002346 Printed in the United Kingdom

A geophysical-scale model of vertical natural convection boundary layers

ANDREW J. WELLS AND M. GRAE WORSTER

Institute of Theoretical Geophysics, Department of Applied Mathematics and Theoretical Physics, University of Cambridge, Wilberforce Road, Cambridge, CB3 0WA, UK

(Received 6 June 2007 and in revised form 29 April 2008)

A model is developed for turbulent natural convection in boundary layers formed next to isothermal vertical surfaces. A scaling analysis shows that the flow can be described by plume equations for an outer turbulent region coupled to a resolved near-wall laminar flow. On the laboratory scale, the inner layer is dominated by its own buoyancy and the Nusselt number scales as the one-third power of the Rayleigh number ($Nu \propto Ra_z^{1/3}$). This gives a constant heat flux, consistent with previous experimental and theoretical studies. On larger geophysical scales the buoyancy is strongest in the outer layer and the laminar layer is driven by the shear imposed on it. The predicted heat transfer correlation then has the Nusselt number proportional to the one-half power of Rayleigh number ($Nu \propto Ra_z^{1/2}$) so that a larger heat flux is predicted than might be expected from an extrapolation of laboratory-scale results. The criteria for transitions between flow regimes are consistent with a hierarchy of instabilities of the near-wall laminar flow, with a buoyancy-driven instability operating on the laboratory scale and a shear-driven instability operating on geophysical scales.

1. Introduction

When a heated, or cooled, vertical plate is introduced into an environment of different temperature, the resulting buoyancy force can drive a predominantly vertical flow adjacent to the plate. This phenomenon is demonstrated by air rising next to a heated radiator or by the motion of water next to a near-vertical ice surface in a polar ocean. This problem has been well studied on the laboratory scale but it is unknown whether these results can be extrapolated to geophysical scales. For example, large tabular icebergs or glacier termini can extend several hundred metres below the surface of oceans or lakes and their melt rate is controlled, in part, by the heat supplied to the ice–water interface. We need an accurate prediction of the heat flux q_w from isothermal surfaces on geophysical scales in order to determine the lifetime of such ice features.

The evolution of heat flux with distance z from the leading edge of a vertical plate is typically described using the dimensionless local Nusselt number

$$Nu_z = \frac{q_w z}{\rho_\infty c_p \kappa \Delta T}, \tag{1.1}$$

where ΔT denotes the temperature difference between plate and ambient, while ρ_∞, c_p and κ denote ambient fluid density, specific heat capacity and thermal diffusivity respectively. Ostrach (1952) presented similarity solutions of the boundary layer equations for laminar flow, and Kuiken (1968) produced an asymptotic breakdown to elucidate the dominant dynamical balances in the limit of large Prandtl number.

The appropriate heat flux variation is found to be

$$Nu_z \propto Ra_z^{1/4}, \tag{1.2}$$

where the local Rayleigh number is defined as

$$Ra_z = g' z^3 / \kappa \nu, \tag{1.3}$$

ν is the kinematic viscosity of the fluid, and

$$g' = g\,(\rho_\infty - \rho_w)\,/\rho_\infty \tag{1.4}$$

is the reduced gravity based on density differences between fluid at the ambient and wall temperatures. This gives a heat flux variation $q_w \propto z^{-1/4}$, decreasing with distance from the leading edge.

For longer surfaces, the flow develops an instability (Nachtsheim 1963; Hieber & Gebhart 1971) and eventually becomes turbulent at a sufficiently large distance from the leading edge. Studies of the instability and the resultant turbulent flow have been summarized by Papailiou (1991). Laboratory-based experimental studies have suggested that the turbulent heat flux is described by

$$Nu_z \propto Ra_z^{1/3} \tag{1.5}$$

for moderate z (e.g. Tsuji & Nagano 1988*a*), which gives a heat flux independent of z over the turbulent region.

There is no formal theoretical solution for turbulent flow. George & Capp (1979) and Hölling & Herwig (2005) attempted to model the flow using asymptotic and dimensional arguments with an inner viscous sublayer, intermediate buoyant layer and an outer inertial region and recovered the constant-heat-flux scaling. An alternative approach has been to define an eddy viscosity to model turbulent Reynolds stresses, and an eddy diffusivity to model turbulent heat flux. Solutions can then be found to the resulting advection–diffusion equation. Josberger & Martin (1981) found $Nu \propto Ra_z^{1/4}$ close to the transition region using eddy diffusivities dependent on the laminar similarity variable, while Ruckenstein (1998) recovered the one-third power law using a scaling argument with eddy diffusivities dependent on distance from the wall. However, Tsuji & Nagano (1988*b*) had previously shown that the eddy viscosity required to explain their experimental results would be negative near to the wall, which is physically disturbing.

There are no experimental studies relevant to the larger geophysical scales. We present a model that suggests the possibility of a second transition in the flow, which may be appropriate to these larger geophysical length scales and gives rise to a different dependence between Nusselt and Rayleigh numbers. The asymptotic limit of our model, beyond the second transition, is consistent with previous *ad hoc* formulations of turbulent convective boundary layers and wall plumes. It puts these on a firmer foundation and determines the parameter ranges in which they are appropriate.

We approach this problem by scaling the governing boundary layer equations and developing a simplified model for a flow split into distinct dynamical regimes. We discuss the key physical balances in § 2 and summarize the key results in each flow regime. We find that the flow can be divided into three regions: an outer inertial turbulent region; an intermediate turbulent viscous layer where molecular diffusivities are important; and a further laminar conductive sublayer resolved within the inner viscous region. The width of the conductive sublayer depends on the dominant force balance in the inner region. If the inner layer is buoyancy-driven then the sublayer width is given in terms of a buoyant instability criterion. Alternatively, the outer layer

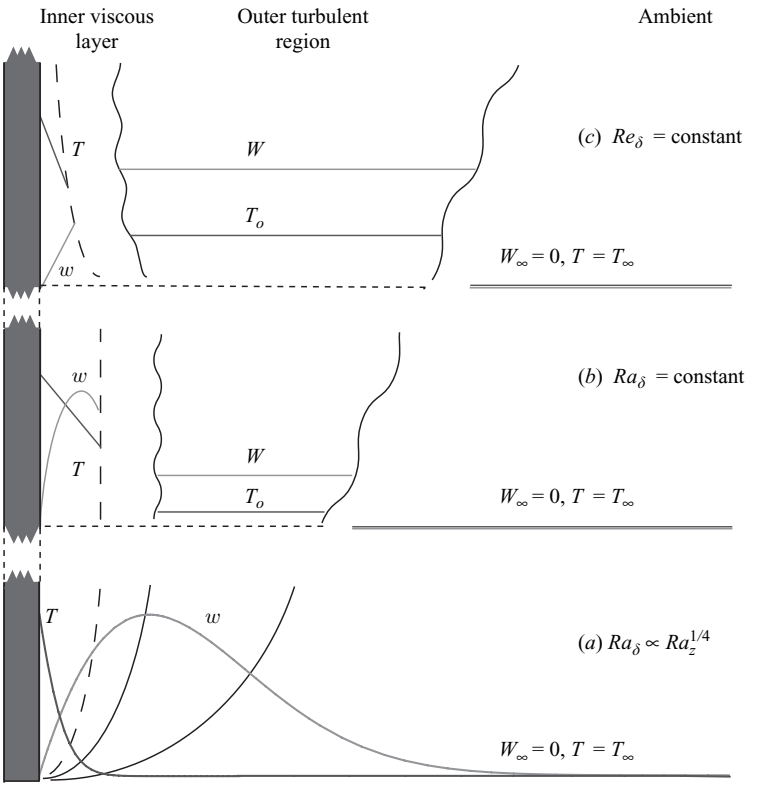

FIGURE 1. Schematic illustration of the dominant force balances present in each of the flow regimes for large *Pr* flow. The boundary layer can be broken down into three sublayers. Viscous forces and conduction dominate the near-wall layer. The intermediate layer is dominated by viscous forces with heat transfer by either advection or turbulent eddy flux. The outer region is dominated by inertia. We observe different flow regimes as the dynamical balance in each region changes. (*a*) Close to the leading edge there is laminar flow, with an inner viscous–buoyancy balance, and outer viscous–inertia balance. (*b*) At intermediate heights we have turbulent flow. The laminar inner layer is buoyancy-driven, with an outer inertial turbulent flow. The laminar inner layer width is consistent with a buoyant instability criterion. (*c*) At large heights we have outer turbulent flow with a buoyancy–inertia balance. The laminar inner layer is shear-driven and the inner layer width is consistent with a shear instability criterion. For the turbulent flow in regions (*b*) and (*c*) W corresponds to the mean vertical velocity, with T_o being the mean temperature, both averaged over the width of the outer turbulent part of the flow.

can become sufficiently buoyant so as to exert a shear that provides the dominant forcing mechanism for the inner flow. In this case the sublayer width satisfies a shear instability criterion. The dominant force balances are shown schematically in figure 1.

These ideas are justified in § 3 using a scaling analysis of the full boundary layer equations to identify each of the physical balances formally. We then derive modelled governing equations in § 4, resolving velocity and temperature fields in the conductive sublayer and using integral balances of mass, momentum and heat across the remainder of the flow. The model is closed in § 5 by applying conditions based on scaling for the entrainment velocity and the shear stress and heat flux between the two layers, giving a system of ordinary differential equations for the averaged properties of the outer flow. This is equivalent to specifying a turbulence closure. Solutions of these equations are presented in § 6 showing the transition between the two distinct

turbulent regimes. Immediately after transition the inner layer is driven by buoyancy, reproducing the constant heat flux scaling (1.5). At larger heights the buoyancy in the outer region grows to dominate the forcing and the inner flow is driven by shear. We show that this recovers a plume model similar to that used by Ellison & Turner (1959) but with the heat flux linearly related to the local plume velocity and the temperature difference from the wall. This model gives the scaling law

$$Nu_z \propto Ra_z^{1/2}, \tag{1.6}$$

and a heat flux that increases in proportion to $z^{1/2}$.

2. Physical outline

We first describe the principal physical interpretation of our analytical results in order to give context to the detailed analysis. The flow is driven by buoyancy, and we obtain different flow regimes depending on the location of the dominant buoyancy force within the boundary layer, as illustrated in figure 1.

Close to the leading edge of the heated surface (region (*a*) of figure 1), the flow is laminar and well understood (Ostrach 1952; Kuiken 1968). For large Prandtl number, the inner layer has a balance between viscous and buoyancy forces, and between conduction and advection of heat. The temperature reaches its ambient value at the edge of the inner layer, so that there is negligible heat transport or buoyancy in the outer layer, where the momentum balance is between viscous and inertial forces. Kuiken (1968) showed that the width of the inner layer scales as

$$\delta_i \propto zRa_z^{-1/4}. \tag{2.1}$$

This shows that a local Rayleigh number, based on the width of the inner layer, is

$$Ra_{\delta_i} \propto Ra_z^{1/4}. \tag{2.2}$$

The laminar boundary layer becomes unstable when the global Rayleigh number Ra_z exceeds a critical value of approximately $1.4 \times 10^5 Pr^2$ (Hieber & Gebhart 1971). Alternatively, we can interpret this as saying that an instability occurs when the local Rayleigh number Ra_{δ_i} exceeds a critical value of about $20Pr^{1/2}$ at some height above the leading edge. This idea is consistent with the first turbulent regime (region (*b*) of figure 1) suggested by the scaling analysis in § 3 below, in which we find that the condition

$$Ra_{\delta_i} = \text{constant} \tag{2.3}$$

determines the width of an inner laminar sublayer. This is suggestive that the width of the inner laminar layer in this regime is controlled by a buoyant instability.

The structure of this turbulent boundary layer has been well studied in laboratory-scale experiments. Tsuji & Nagano (1988*b*) made detailed measurements of the temperature and velocity profiles and turbulent fluxes for a boundary layer next to a heated plate in air. These measurements show that we can consider a multi-layered structure to the boundary layer for turbulent flow. Conduction of heat and viscous forces dominate very close to the wall, with the turbulent eddy fluxes beginning to become important as we move further from the wall. The laboratory-scale measurements suggest buoyancy forces are important across both of these inner regions. Finally, molecular conduction and viscous forces become small at large distances from the wall, with advection and inertia now balancing the turbulent fluxes of heat and momentum. These observations are also consistent with the scaling ideas of George & Capp (1979)

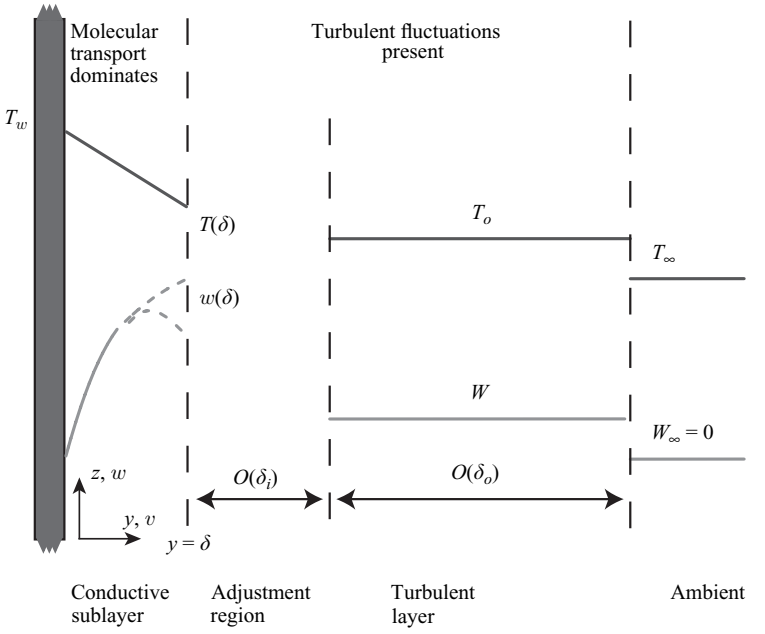

FIGURE 2. Schematic illustration of the structure of the boundary layer. Close to the wall we have a laminar conductive sublayer for $0 < y < \delta$. The outer region of the flow has width $O(\delta_o)$, is fully turbulent and is dominated by inertia. We also have an intermediate viscous-turbulent layer of width $O(\delta_i)$ where the flow adjusts between the near wall and outer regions. Since $\delta_o \gg \delta_i \gg \delta$, these boundary layer scales can be measured either as distance from the wall, or from the edge of the neighbouring region. As indicated by the alternative dashed profiles in the inner region, the flow there either exerts a shear on the outer layer, or is driven by shear from the outer layer.

and Hölling & Herwig (2005), who identified an inner 'constant heat flux layer' which was dominated by buoyancy. We show in the scaling analysis of § 3 that this multi-layered structure can be considered as the three distinct regions shown in figure 2.

We have an inner layer of width δ near to the wall, in which heat transport is entirely conductive and the dominant momentum balance is between laminar viscosity and buoyancy forces.

Further from the wall, we introduce an intermediate viscous–turbulent layer, of width $O(\delta_i)$. Turbulent eddy structures begin to influence the heat transfer in this region, although viscous forces still dominate inertia.

Finally, we have an outer inertial–turbulent region of width $O(\delta_o)$. Molecular transport is negligible in this region, and the vigorous turbulence keeps it relatively well mixed, with fluid engulfed from the ambient at the edge of the layer.

With this multi-layer structure in mind, we now return to consider the development of the turbulent flow in figure 1. We find that as z increases buoyancy spills from the inner to the outer layer, which suggests a new possibility that the buoyancy in the outer layer can grow to dominate the flow, as shown in region (c) of figure 1. The inner layer is then driven by the shear exerted by the outer flow, and we find that the inner layer width δ_i satisfies

$$Re_{\delta_i} = \frac{W\delta_i}{\nu} = \text{constant}, \tag{2.4}$$

so that there is a constant local Reynolds number (rather than Rayleigh number) characterizing the flow. This is consistent with the idea that the inner laminar sublayer

width is controlled by a shear instability. The complete evolution of the inner layer width is described by a hierarchy of instabilities, with the laminar criterion (2.2) initially giving way to a buoyant instability criterion (2.3), before finally satisfying a shear instability criterion (2.4) when the outer velocity becomes large, as depicted in figure 1.

These physical ideas form the basis of the unified model displayed in table 1 at the start of § 6. Sections 3–5 provide a formal justification for the mathematical model: the reader interested primarily in the application of this model could jump straight to § 6.

3. Scaling analysis

The physical ideas discussed in § 2 and illustrated in figure 2 suggest the role of multiple sublayers, with changes in the overall flow pattern depending on the dynamical balance in each. We will determine the length scales of each of these regions by considering different asymptotic limits of the governing equations.

The Reynolds-averaged Boussinesq boundary layer equations for thermally buoyant flow next to a vertical isothermal plate are

$$\frac{\partial v}{\partial y} + \frac{\partial w}{\partial z} = 0, \tag{3.1}$$

$$v\frac{\partial w}{\partial y} + w\frac{\partial w}{\partial z} = \nu\frac{\partial^2 w}{\partial y^2} + g\alpha(T - T_\infty) - \frac{\partial}{\partial y}(\overline{v'w'}), \tag{3.2}$$

$$v\frac{\partial T}{\partial y} + w\frac{\partial T}{\partial z} = \kappa\frac{\partial^2 T}{\partial y^2} - \frac{\partial}{\partial y}(\overline{v'T'}), \tag{3.3}$$

where (v, w, T) are the ensemble-averaged mean horizontal velocity, vertical velocity and temperature, and (v', w', T') the corresponding turbulent fluctuations about the mean state (see Gebhart *et al.* 1988, for example). The ensemble average of a quantity ξ is denoted by $\overline{\xi}$. The thermal expansion coefficient is denoted by α. These equations are subject to boundary conditions

$$v = w = 0, \quad T = T_w \quad \text{at} \quad y = 0, \tag{3.4}$$

$$T \to T_\infty, \quad w,\ v'w',\ v'T' \to 0 \quad \text{as} \quad y \to \infty, \tag{3.5}$$

corresponding to a fixed isothermal surface and uniform conditions far from the wall.

We non-dimensionalize these equations by defining

$$\left.\begin{gathered}(v, w) = (\mathscr{V}\hat{v}, \mathscr{W}\hat{w}), \quad T - T_\infty = \Delta\mathscr{T}\hat{\theta}, \quad (y, z) = (\mathscr{D}\hat{y}, \mathscr{L}\hat{z},), \\ (v', w') = (\mathscr{V}'\hat{v}', \mathscr{W}'\hat{w}'), \quad T' = \mathscr{T}'\hat{\theta}',\end{gathered}\right\} \tag{3.6}$$

where $(\mathscr{V}, \mathscr{W}, \mathscr{V}', \mathscr{W}')$ are characteristic velocity scales, $(\Delta\mathscr{T}, \mathscr{T}')$ are temperature and temperature fluctuation scales and $(\mathscr{D}, \mathscr{L})$ are length scales. Scaling of the incompressibility relation (3.1) gives

$$\frac{\mathscr{V}}{\mathscr{D}}\frac{\partial\hat{v}}{\partial\hat{y}} + \frac{\mathscr{W}}{\mathscr{L}}\frac{\partial\hat{w}}{\partial\hat{z}} = 0, \quad \Rightarrow \quad \mathscr{V} = \frac{\mathscr{D}}{\mathscr{L}}\mathscr{W}. \tag{3.7}$$

This can be used to give scalings of the momentum equation

$$\frac{\mathscr{W}^2}{\mathscr{L}}\hat{\boldsymbol{u}}\cdot\hat{\nabla}\hat{w} = g\alpha\Delta\mathscr{T}\hat{\theta} + \frac{\nu\mathscr{W}}{\mathscr{D}^2}\hat{w}_{\hat{y}\hat{y}} - \frac{\mathscr{V}'\mathscr{W}'}{\mathscr{D}}(\hat{\overline{v'w'}})_{\hat{y}}, \tag{3.8}$$

and the heat equation

$$\frac{\mathscr{W}\Delta\mathscr{T}}{\mathscr{L}}\hat{\boldsymbol{u}}\cdot\hat{\boldsymbol{\nabla}}\hat{\theta}=\frac{\kappa\Delta\mathscr{T}}{\mathscr{D}^2}\hat{\theta}_{\hat{y}\hat{y}}-\frac{\mathscr{V}'\mathscr{T}'}{\mathscr{D}}(\widehat{\overline{v'\theta'}})_{\hat{y}}. \tag{3.9}$$

The horizontal length scale $\mathscr{D}$ takes a different value δ, δ_i or δ_o in each region where we have a different dynamical balance. If $\mathscr{D}$ satisfies

$$\frac{\mathscr{D}}{\mathscr{L}}\ll\min\left\{\left(\frac{\mathscr{W}\mathscr{L}}{\nu}\right)^{1/2},\ \left(\frac{\mathscr{W}\mathscr{L}}{\kappa}\right)^{1/2},\ \left(\frac{\kappa\Delta\mathscr{T}}{\mathscr{L}\mathscr{V}'\mathscr{T}'}\right),\ \left(\frac{\nu\mathscr{W}}{\mathscr{L}\mathscr{V}'\mathscr{W}'}\right)\right\}, \tag{3.10}$$

then we have a laminar, conductive sublayer, where the dominant balances are given by

$$\nu\frac{\partial^2 w}{\partial y^2}+\alpha g(T-T_\infty)\approx 0, \tag{3.11}$$

$$\kappa\frac{\partial^2 T}{\partial y^2}\approx 0, \tag{3.12}$$

with next-order corrections at $O(\mathscr{D}/\mathscr{L})$. The balances (3.11) and (3.12) maintain the same form in the inner layer of each of the flow regimes. Viscous forces and also possibly buoyancy forces are present in the momentum balance (3.11). The heat conducted into the layer at $y=0$ is conducted out of the layer at the opposite edge, so this is a constant flux layer, consistent with the models of George & Capp (1979) and Hölling & Herwig (2005).

Further away from the wall, $\mathscr{D}$ is larger, one of the conditions in (3.10) fails and a new dynamical balance becomes important. The intermediate length scale δ_i is given by the value of $\mathscr{D}$ that generates the first failure of (3.10). We will also determine an outer length scale δ_o by considering the dominant dynamical balance in the outer region of the flow.

The scalings δ_i and δ_o vary depending on whether the flow is laminar, turbulent with a buoyant inner layer or turbulent with an inner layer driven by shear. The scales also depend on the Prandtl number $Pr=\nu/\kappa$. We first develop scalings for flows with $Pr\geqslant O(1)$, relevant to most geophysical applications (typically, $Pr=0.7$ for air, and $Pr\approx 10$ for cold sea water), and then generalize them to small Prandtl number.

3.1. *Scaling for laminar flow*

As a consistency check, we use our scaling analysis to reproduce the length scales for large Pr determined asymptotically by Kuiken (1968).

The turbulent fluctuation terms are absent for laminar flow, and so the viscous and thermal boundary layer thicknesses represent the two relevant length scales. The viscous boundary layer thickness is determined by the extent to which viscous shear acts on the flow in the momentum equation. Similarly, the thermal boundary layer thickness is determined by the length scale for conduction of heat. If $Pr\geqslant 1$ then $\nu\geqslant\kappa$, and viscous forces diffuse momentum over a length scale at least as large as that of thermal diffusion. Hence, we expect the inner length scale δ_i to be determined by the balance of advection and diffusion of heat in (3.9), giving

$$\frac{\mathscr{W}\Delta\mathscr{T}}{\mathscr{L}}\sim\frac{\kappa\Delta\mathscr{T}}{\delta_i^2}. \tag{3.13}$$

The buoyancy force is only generated in regions where there is a temperature difference from the ambient, and hence it is confined to the thermal boundary layer,

as shown schematically in figure 1(*a*). The balance of buoyancy and viscous forces in (3.8) gives

$$g\alpha\Delta\mathscr{T} \sim \frac{\nu\mathscr{W}}{\delta_i^2}. \tag{3.14}$$

This can be used to eliminate $\mathscr{W}$ from (3.13) to give

$$\frac{\delta_i}{\mathscr{L}} \sim \left(\frac{g\alpha\Delta\mathscr{T}\mathscr{L}^3}{\kappa\nu}\right)^{-1/4} \equiv Ra_{\mathscr{L}}^{-1/4}. \tag{3.15}$$

Outside the thermal boundary layer $\hat{\theta} \ll 1$, and so the heat equation does not provide any useful information. In addition, the buoyancy force no longer produces a significant contribution to the flow, and hence the outer inertia balances the viscous shear generated by the inner flow. The balance of inertia and viscous terms in (3.8) gives the outer flow length scale δ_o from

$$\frac{\mathscr{W}^2}{\mathscr{L}} \sim \frac{\nu\mathscr{W}}{\delta_o^2} \qquad \Rightarrow \qquad \frac{\delta_o}{\mathscr{L}} \sim Pr^{1/2}\frac{\delta_i}{\mathscr{L}} \propto Pr^{1/2}Ra_{\mathscr{L}}^{-1/4}. \tag{3.16}$$

These scalings match those derived asymptotically by Kuiken (1968). We expect them to persist until the laminar flow becomes unstable when $Ra_z \approx 1.4 \times 10^5 Pr^2$ (as given for large Pr by Hieber & Gebhart 1971) and the turbulent fluctuation terms begin to grow.

3.2. *Scaling for turbulent flow*

The presence of turbulent fluctuations allows a new scaling balance to develop. For large Prandtl number we expect the thermal boundary layer to be narrower than the viscous boundary layer, so that δ_i will again be determined by the heat equation. Far from the wall, where $\mathscr{D}/\mathscr{L} \gg (\kappa/\mathscr{W}\mathscr{L})^{1/2}$, conduction of heat is negligible and the balance in (3.9) is between advection and turbulent fluctuations, giving

$$\frac{\mathscr{W}\Delta\mathscr{T}}{\mathscr{L}} \sim \frac{\mathscr{V}'\mathscr{T}'}{\delta_o}. \tag{3.17}$$

This is consistent with the experimental findings of Tsuji & Nagano (1988 *b*), who observed an outer turbulent flow dominated by advection and turbulent transport of heat, with turbulent fluctuations penetrating into an inner conductive region.

The intermediate heat balance (3.9) can then be written as

$$\hat{\theta}_{\hat{y}\hat{y}} - \frac{\delta_i\mathscr{V}'\mathscr{T}'}{\kappa\Delta\mathscr{T}}(\widehat{\overline{v'\theta'}})_{\hat{y}} = \frac{\mathscr{W}\delta_i^2}{\kappa\mathscr{L}}\hat{\boldsymbol{u}}\cdot\hat{\nabla}\hat{\theta}. \tag{3.18}$$

Assuming that the turbulent fluctuations are of the same magnitude in both intermediate and outer layers, given by the scaling (3.17), we see that

$$\frac{\delta_i\mathscr{V}'\mathscr{T}'}{\kappa\Delta\mathscr{T}} \sim \frac{\mathscr{W}\delta_i\delta_o}{\kappa\mathscr{L}} \qquad \Rightarrow \qquad \frac{\delta_i\mathscr{V}'\mathscr{T}'}{\kappa\Delta\mathscr{T}} \gg \frac{\mathscr{W}\delta_i^2}{\kappa\mathscr{L}} \tag{3.19}$$

and so, in the intermediate layer, turbulent fluctuations must balance conduction at leading order, again consistent with experimental observation (Tsuji & Nagano 1988 *b*). The intermediate length scale therefore satisfies

$$\frac{\mathscr{W}\delta_i}{\kappa} \sim \frac{\mathscr{L}}{\delta_o}. \tag{3.20}$$

The outer layer width δ_o is determined by the outer momentum balance and turbulent entrainment characteristics. The Reynolds stresses balance inertia in the

outer region, giving

$$\frac{\mathscr{V}'\mathscr{W}'}{\delta_o} \sim \frac{\mathscr{W}^2}{\mathscr{L}}. \tag{3.21}$$

Incompressibility (3.7) yields

$$\frac{\mathscr{V}}{\mathscr{W}} \sim \frac{\mathscr{V}'}{\mathscr{W}'} \sim \frac{\delta_o}{\mathscr{L}}, \tag{3.22}$$

which can be combined with (3.21) to give

$$\mathscr{W}' \sim \mathscr{W}, \quad \mathscr{V}' \sim \mathscr{V}. \tag{3.23}$$

There are no other independent velocity scales in the outer flow (if the outer buoyancy is important then $\mathscr{W}$ will be defined by a balance between inertia and buoyancy) and so we must have

$$\frac{\delta_o}{\mathscr{L}} = E, \tag{3.24}$$

for some constant E, possibly dependent on Pr. We will see later that this is consistent with the entrainment hypothesis for turbulent flows suggested by Morton, Taylor & Turner (1956). The intermediate layer width is then given by

$$\frac{\mathscr{W}\delta_i}{\kappa} \sim \frac{1}{E} = \text{constant}. \tag{3.25}$$

This is consistent with the experimental observation of Kutateladze, Kirdyashkin & Ivakin (1972), who found that at any given z the velocity maximum $W_{\max}$ and its distance from the plate δ_1 satisfy

$$Re_1 Pr^{1/2} \equiv \frac{W_{\max}\delta_1}{(\nu\kappa)^{1/2}} = \text{constant}. \tag{3.26}$$

The condition (3.25) can take on two forms dependent on the velocity scale $\mathscr{W}$, which is determined by the dominant force balance in the intermediate layer.

3.2.1. *Buoyancy-driven inner layer*

When the inner region is driven by buoyancy there is a balance of viscous and buoyancy forces in the intermediate layer,

$$g\alpha\Delta\mathscr{T} \sim \frac{\nu\mathscr{W}}{\delta_i^2}. \tag{3.27}$$

Eliminating $\mathscr{W}$ from (3.25), we obtain

$$Ra_{\delta_i} \equiv \frac{g\alpha\Delta\mathscr{T}\delta_i^3}{\kappa\nu} \sim \frac{1}{E} = \text{constant}. \tag{3.28}$$

We might think of the inner viscous layer width being determined by a buoyant instability condition in terms of a local Rayleigh number based on δ_i. We have laminar flow close to the wall for $y \ll \delta_i$ with an instability generating turbulent fluctuations when $y \sim \delta_i$.

3.2.2. *Shear-driven inner layer*

We shall see from our model results that as the flow develops along the wall, buoyancy spills from the inner to the outer layer. If the buoyancy in the outer layer becomes sufficiently large, large outer velocities are generated which then exert a shear force on the inner layer. If the shear force dominates the buoyancy from the

inner layer, then $\mathscr{W}$ will scale with the outer velocity. Hence, we might interpret (3.25) as an intermediate layer width determined by a shear instability condition, described in terms of a local Reynolds number

$$Re_{\delta_i} \equiv \frac{\mathscr{W}\delta_i}{\nu} \sim \frac{1}{EPr} = \text{constant}. \tag{3.29}$$

The inner region develops as a shear flow driven by the imposed outer inertial velocity, with turbulent fluctuations now controlled by shear instability. The shear criterion replaces the buoyant instability criterion whenever

$$\frac{\nu\mathscr{W}}{\delta_i} \gg g'\delta_i. \tag{3.30}$$

This all suggests the possibility of a hierarchy of instability conditions, as shown schematically in figure 1. Initially there is laminar flow, with $\delta_i \propto zRa_z^{-1/4}$ growing with height z until a buoyant instability is triggered at some critical value of Ra_{δ_i}. The flow then develops in this buoyant instability turbulent regime until the outer velocity $\mathscr{W}$ grows sufficiently large for a shear instability mechanism to dominate at some critical value of Re_{δ_i}.

3.3. *Scalings for small Prandtl number*

For $Pr < 1$, the viscous length scale is smaller than the thermal length scale, and so the scalings differ slightly. In the outer flow, inertia balances the Reynolds stresses,

$$\frac{\mathscr{W}^2}{\mathscr{L}} \sim \frac{\mathscr{V}'\mathscr{W}'}{\delta_o}. \tag{3.31}$$

The intermediate layer width is determined by the balance between viscous forces and the Reynolds stresses, giving

$$\frac{\nu\mathscr{W}}{\delta_i^2} \sim \frac{\mathscr{V}'\mathscr{W}'}{\delta_i} \tag{3.32}$$

and so the criterion (3.25) for the width of the intermediate layer is replaced by

$$\frac{\mathscr{W}\delta_i}{\nu} \sim \frac{1}{E}. \tag{3.33}$$

The derivation then continues as before, adjusted by the appropriate factor of Pr.

4. General governing equations for a two-layer flow

Guided by the preceding scaling analysis, we now develop appropriate governing equations for an inner laminar conductive sublayer ($y < \delta$) and an outer flow region ($y > \delta$), where δ is a specific numerical value at which flow properties are matched.

4.1. *The laminar conductive sublayer*

The scaling analysis suggests that the laminar conductive sublayer is described by equations (3.1), (3.11) and (3.12), with heat transfer via conduction only, and viscous and buoyancy forces dominating the momentum balance. Incompressibility is satisfied by use of a streamfunction ψ, with $v = -\psi_z$ and $w = \psi_y$. This yields the ordinary differential equations

$$T_{yy} = 0, \tag{4.1}$$

$$\psi_{yyy} + \frac{\alpha g}{\nu}(T - T_\infty) = 0, \tag{4.2}$$

$$\psi = \psi_y = 0, \quad T = T_w \quad \text{at} \quad y = 0, \tag{4.3}$$

$$\nu\psi_{yy} = \frac{\tau}{\rho_\infty}, \quad -\kappa T_y = \frac{q}{\rho_\infty c_p} \quad \text{at} \quad y = \delta, \tag{4.4}$$

for $0 < y < \delta$. The boundary conditions at $y = 0$ correspond to no slip and no normal flow at the isothermal surface, and those at $y = \delta$ correspond to matching of shear stress τ and heat flux q to the outer layer. The variables τ and q will be determined later. This system has solution

$$T - T_\infty = T_w - T_\infty - \frac{q}{\rho_\infty c_p \kappa} y, \tag{4.5}$$

$$\psi = \frac{\tau}{\rho_\infty \nu} \frac{y^2}{2} + \frac{g' y^2}{\nu} \left[\frac{3\delta - y}{6} - \frac{q}{\rho_\infty c_p \kappa (T_w - T_\infty)} \left(\frac{6\delta^2 - y^2}{24} \right) \right], \tag{4.6}$$

and hence

$$w = \frac{\tau}{\rho_\infty \nu} y + \frac{g' \delta y}{\nu} \left[1 - \frac{y}{2\delta} - \frac{q\delta}{\rho_\infty c_p \kappa (T_w - T_\infty)} \left(\frac{1}{2} - \frac{y^2}{6\delta^2} \right) \right]. \tag{4.7}$$

Note that the temperature gradient is independent of y, giving a constant heat flux across the inner layer, i.e. $q_w = q$. The inner velocity w can be driven by either the buoyancy generated in the inner layer (the term involving g'), or the shear exerted by the outer layer (the term involving τ).

4.2. *The outer turbulent region*

Turbulent free-convection flows have been successfully modelled by the plume equations of Morton *et al.* (1956), and a similar approach was used by Ellison & Turner (1959) to model wall-bounded density currents. They integrated the turbulent boundary layer equations over a cross-section, deriving ordinary differential equations in z for the average mass, momentum and buoyancy fluxes. We follow a similar approach, but instead integrate the boundary layer equations (3.1)–(3.3) over the range $\delta \leqslant y < \infty$. The boundary conditions for the outer turbulent section of the flow are

$$v = v(\delta, z), \quad \rho_\infty \nu w_y = \tau(\delta, z), \quad -\rho_\infty c_p \kappa T_y = q(\delta, z), \tag{4.8}$$

$$T \to T_\infty, \quad w,\ v'w',\ v'T' \to 0 \quad \text{as} \quad y \to \infty, \tag{4.9}$$

equivalent to uniform conditions at large distances from the wall.

Assuming that the mean flow is steady and that the ambient temperature field is unstratified, we derive the integrated equations

$$\frac{\mathrm{d}}{\mathrm{d}z} \left(\int_\delta^\infty w \, \mathrm{d}y \right) = [-v]_\delta^\infty, \tag{4.10}$$

$$\frac{\mathrm{d}}{\mathrm{d}z} \left(\int_\delta^\infty w^2 \, \mathrm{d}y \right) = \int_\delta^\infty g\alpha \, (T - T_\infty) \, \mathrm{d}y - \frac{\tau}{\rho_\infty}, \tag{4.11}$$

$$\frac{\mathrm{d}}{\mathrm{d}z} \left(\int_\delta^\infty w(T - T_\infty) \, \mathrm{d}y \right) = \frac{q}{\rho_\infty c_p}, \tag{4.12}$$

where

$$\frac{\tau}{\rho_\infty} = \left[\nu \frac{\partial w}{\partial y} - \overline{v'w'} \right]_{y=\delta} \tag{4.13}$$

is the downward shear exerted by the inner viscous flow on the outer flow at $y = \delta$, and

$$\frac{q}{\rho_\infty c_p} = \left[-\kappa \frac{\partial T}{\partial y} + \overline{v'T'}\right]_{y=\delta} \tag{4.14}$$

is the heat flux from the inner layer to the outer layer. We have assumed that the variation of the sublayer width δ is much slower than the variation in outer flow properties, that is,

$$\frac{\mathrm{d}\delta}{\mathrm{d}z} \ll \frac{1}{w}\frac{\mathrm{d}}{\mathrm{d}z}\left(\int_\delta^\infty w \,\mathrm{d}y\right) \quad \text{and} \quad \frac{\mathrm{d}\delta}{\mathrm{d}z} \ll \frac{1}{wT}\frac{\mathrm{d}}{\mathrm{d}z}\left(\int_\delta^\infty wT \,\mathrm{d}y\right), \tag{4.15}$$

so that the limits of integration can be treated as effectively constant with respect to the outer flow.

We can specify the volume, momentum and buoyancy fluxes in terms of an effective mean plume width, b, vertical velocity, W, and temperature T_o, which are defined by

$$bW = \int_\delta^\infty w \,\mathrm{d}y, \tag{4.16}$$

$$bW^2 = \int_\delta^\infty w^2 \,\mathrm{d}y, \tag{4.17}$$

$$bW(T_o - T_\infty) = \int_\delta^\infty w(T - T_\infty) \,\mathrm{d}y. \tag{4.18}$$

Equations (4.10)–(4.12) are exact in the limit of slowly varying δ, but we must make further assumptions to gain additional simplification, and to enforce a turbulence closure for the turbulent fluctuations.

We approximate the buoyancy force as

$$\int_\delta^\infty g\alpha(T - T_\infty) \,\mathrm{d}y = bg\alpha(T_o - T_\infty). \tag{4.19}$$

This relation is exact for 'top-hat' profiles which are uniform across the width of the turbulent region. In addition, if the constant αg is modified by multiplication by an appropriate constant shape factor, (4.19) is correct for any self-similar boundary layer profiles (Linden 2000). We will also assume that $v(\delta) \ll v(\infty)$, since horizontal velocities will be small near to the impermeable wall.

Equations (4.5), (4.7) and (4.10)–(4.12) form a system of five equations for the nine unknowns b, W, T_o, $v(\infty)$, τ, q, $w(\delta)$, $T(\delta)$ and δ. The inner layer width δ is determined by the buoyant and shear instability criteria suggested by the scaling analysis. We therefore require three more conditions in order to close the system. Note that this is consistent with the need for a turbulence closure, as the Reynolds-averaged Navier–Stokes equations introduce three new quantities v', w' and T'.

5. Closure via scaling arguments

We use dimensional and scaling arguments to specify τ, q and $v(\infty)$ in terms of the velocity and temperature scales in the inner and outer layers. The structure of the boundary layer is illustrated schematically in figure 2.

For turbulent outer flow, incompressibility yields

$$\mathscr{V} \sim \frac{\delta_o}{\mathscr{L}}\mathscr{W} \sim E\mathscr{W}, \tag{5.1}$$

given the scaling relation (3.24). Hence, we approximate the entrainment velocity as

$$v(\infty) = -EW. \tag{5.2}$$

This is consistent with the entrainment assumption of Morton *et al.* (1956). The use of an entrainment constant was also justified for wall-bounded density currents by the filling box experiments of Wells & Wettlaufer (2005). For laminar flow, (3.16) instead gives

$$\frac{\delta_o}{\mathscr{L}} = E_1 Pr^{1/2} Ra_z^{-1/4} \quad \Rightarrow \quad v(\infty) = -E_1 Pr^{1/2} Ra_z^{-1/4} W, \tag{5.3}$$

where E_1 is a constant of proportionality, and we have here identified $\mathscr{L} = z$ as the vertical length scale.

The heat flux at $y = \delta$ is given by

$$\frac{q}{\rho_\infty c_p} = \left[-\kappa \frac{\partial T}{\partial y} + \overline{v'T'} \right]_{y=\delta}.$$

This is made up of two components: conductive and turbulent heat fluxes. The temperature must undergo an adjustment from the inner conductive sublayer temperature $T(\delta)$ to the outer temperature T_o over the region of width $O(\delta_i)$ where the intermediate scaling is valid. Hence, we approximate the conductive heat flux over this region using

$$-\kappa T_y|_\delta = \beta_1 \frac{\kappa\,[T(\delta) - T_o]}{\delta}, \tag{5.4}$$

for some constant β_1. In the outer layer, the turbulent fluctuation heat flux scales as

$$(\overline{v'T'})_y \sim vT_y \sim wT_z \quad \Rightarrow \quad \overline{v'T'} \sim \frac{\delta_o}{\mathscr{L}} \mathscr{W}\,[T_o - T(\delta)]\,. \tag{5.5}$$

We expect heat to flow from hot regions to colder regions, and so we set

$$\overline{v'T'}\big|_\delta = \beta_2 \frac{\delta_o}{\mathscr{L}} |W|\,[T(\delta) - T_o]\,, \tag{5.6}$$

for some constant β_2. This gives the total heat flux as

$$\frac{q}{\rho_\infty c_p} = \beta_1 \frac{\kappa\,[T(\delta) - T_o]}{\delta} + \beta_2 \frac{\delta_o}{\mathscr{L}} |W|\,[T(\delta) - T_o]\,. \tag{5.7}$$

The shear stress τ can be found by using similar scaling arguments. We have

$$\frac{\tau}{\rho_\infty} = \left[\nu \frac{\partial w}{\partial y} - \overline{v'w'} \right]_{y=\delta}. \tag{5.8}$$

The velocity must adjust from the sublayer value $w(\delta)$ to the outer value W over the intermediate region of width $O(\delta_i)$. Hence we approximate

$$\nu w_y|_\delta = \gamma_1 \frac{\nu\,[W - w(\delta)]}{\delta}. \tag{5.9}$$

The turbulent Reynolds stress contribution scales according to

$$(\overline{v'w'})_y \sim vw_y \sim ww_z \tag{5.10}$$

and so we let

$$\overline{v'w'}|_\delta = \gamma_2 \frac{\delta_o}{\mathscr{L}} |W|\,[W - w(\delta)]\,, \tag{5.11}$$

where the absolute value has been chosen so that a faster-moving inner layer will exert an upward shear on a slower-moving outer layer. Here γ_1 and γ_2 are arbitrary constants. This gives a total shear stress

$$\frac{\tau}{\rho_\infty} = \gamma_1 \frac{\nu\,[W - w(\delta)]}{\delta} + \gamma_2 \frac{\delta_o}{\mathscr{L}} |W|\,[W - w(\delta)]\,. \tag{5.12}$$

The same scalings apply in the laminar regime, provided the turbulent fluxes are removed by setting $\beta_2 = \gamma_2 = 0$.

The model is completed by the specification of the extent of the conductive sublayer, δ. Following the scaling analysis of § 3 we set

$$Ra_\delta \equiv \frac{g'\delta^3}{\kappa\nu} = \lambda^3 Ra_z^{1/4}, \tag{5.13}$$

for laminar flow, with λ a constant of proportionality. When a critical value of Ra_z is exceeded we have a transition to turbulent flow, and we set

$$Ra_\delta = Ra_c \quad \text{for} \quad \frac{W}{\nu}\left(\frac{\kappa\nu Ra_c}{g'}\right)^{1/3} < Re_c, \tag{5.14}$$

$$Re_\delta \equiv \frac{W\delta}{\nu} = Re_c \quad \text{for} \quad \frac{W}{\nu}\left(\frac{\kappa\nu Ra_c}{g'}\right)^{1/3} > Re_c, \tag{5.15}$$

corresponding to an inner-layer width determined by the buoyant instability criterion until the outer velocity grows enough for the shear instability criterion to dominate.

6. Solutions of the closed model for outer flow

The complete set of governing equations are summarized in table 1.

We shall integrate the closed equations (6.3)–(6.14) to determine the evolution of the flow, and compare the results to the experimental data of Tsuji & Nagano (1988*a*, *b*).

There are several unknown constants in the model. The constants β_1 and γ_1 represent laminar transport properties, β_2 and γ_2 represent corresponding turbulent transport properties and E_1 and E_2 represent laminar and turbulent entrainment strengths; λ, Ra_c and Re_c fix the extent of the laminar conductive sublayer in each regime, and control the transitions between the regimes. It might be thought at this point that a theory with nine adjustable parameters is simply an elaborate scheme for curve fitting. However we fix E_1, β_1 and γ_1 in terms of λ by comparing our integrated model results to the full analytical similarity solution of Kuiken (1968). We estimate Re_c by analogy with the instability of a standard Blasius boundary layer and we estimate the remaining parameters from experimental profiles at a single value of z. With the parameters fixed once and for all, the model is then validated in terms of measured variations of heat flux and shear stress with z.

6.1. *Solution for the laminar regime*

For laminar flow, $\beta_2 = \gamma_2 = 0$ and equations (6.3)–(6.11) have a similarity solution in which

$$b = \frac{4}{3} E_1 Pr^{1/2} \left(\frac{\kappa\nu}{g'}\right)^{1/4} z^{1/4}, \tag{6.15}$$

$$W = W_0 Pr^{-1/2} (g'z)^{1/2}, \tag{6.16}$$

$$T_o - T_\infty = \Theta_0\,(T_w - T_\infty)\,, \tag{6.17}$$

Inner flow ($0 < y < \delta$):

$$w = \frac{\tau y}{\rho_\infty \nu} + \frac{g'\delta^2}{\nu}\left[\frac{y}{\delta} - \frac{y^2}{2\delta^2} - \frac{qy}{\rho_\infty c_p \kappa (T_w - T_\infty)}\left(\frac{1}{2} - \frac{y^2}{6\delta^2}\right)\right], \tag{6.1}$$

$$T - T_\infty = T_w - T_\infty - \frac{q}{\rho_\infty c_p \kappa} y. \tag{6.2}$$

Outer flow ($y > \delta$):

$$\frac{\mathrm{d}}{\mathrm{d}z}[bW] = -v(\infty), \tag{6.3}$$

$$\frac{\mathrm{d}}{\mathrm{d}z}[bW^2] = \alpha g b\,(T_o - T_\infty) - \frac{\tau}{\rho_\infty} \tag{6.4}$$

$$\frac{\mathrm{d}}{\mathrm{d}z}\left[bW\,(T_o - T_\infty)\right] = \frac{q}{\rho_\infty c_p}, \tag{6.5}$$

Matching:

$$v(\infty) = -\frac{\delta_o}{\mathscr{L}} W, \tag{6.6}$$

$$\frac{\tau}{\rho_\infty} = \gamma \frac{\nu}{\delta}\left[W - w(\delta)\right], \tag{6.7}$$

$$\frac{q}{\rho_\infty c_p} = \beta \frac{\kappa}{\delta}\left[T(\delta) - T_o\right], \tag{6.8}$$

$$\beta = \left(\beta_1 + \beta_2 \frac{\delta_o}{\mathscr{L}} \frac{\delta\,|W|}{\kappa}\right), \qquad \gamma = \left(\gamma_1 + \gamma_2 \frac{\delta_o}{\mathscr{L}} \frac{\delta\,|W|}{\nu}\right). \tag{6.9}$$

Laminar scales:

$$\delta = \frac{\lambda z}{Ra_z^{1/4}}, \tag{6.10}$$

$$\frac{\delta_o}{\mathscr{L}} = \frac{E_1 Pr^{1/2}}{Ra_z^{1/4}}. \tag{6.11}$$

Turbulent scales:

$$Ra_\delta = Ra_c = \lambda^3 Ra_t^{1/4}, \quad \frac{W}{\nu}\left(\frac{\kappa \nu Ra_c}{g'}\right)^{1/3} < Re_c \tag{6.12}$$

$$\frac{W\delta}{\nu} = Re_c, \qquad \frac{W}{\nu}\left(\frac{\kappa \nu Ra_c}{g'}\right)^{1/3} > Re_c, \tag{6.13}$$

$$\frac{\delta_o}{\mathscr{L}} = E. \tag{6.14}$$

Asymptotic limits:

Buoyant instability	$10^9 < Ra_z < 10^{16}$,	$Ra_\delta = \text{const.}$	τ negligible,	$\dfrac{q}{\rho_\infty c_p} = \text{const.}$
Shear instability	$10^{16} < Ra_z$,	$Re_\delta = \text{const.}$	$\dfrac{\tau}{\rho_\infty} = K_f W\,\lvert W\rvert$,	$\dfrac{q}{\rho_\infty c_p} = St\,\lvert W\rvert\,(T_w - T_o)$.

TABLE 1. Summary of the governing equations for inner and outer flow in both laminar and turbulent regimes. In the inner layer inertia and advection are negligible and viscous flow is driven by a linear temperature profile. The outer flow is described by equations for a wall plume of width b with average outer velocity W and temperature T_o. The outer and inner flow are coupled via the shear stress τ and heat flux q, which take different asymptotic forms in each of the buoyant instability and shear instability regimes, while K_f and St are proportionality constants.

where W_0 and Θ_0 are dimensionless constants. Using these expressions and (6.1)–(6.11) we obtain, after some algebra,

$$v(\infty) = -E_1 W_0 \left(\frac{g'\kappa\nu}{z}\right)^{1/4}, \tag{6.18}$$

$$\frac{\tau_w}{\rho_\infty} = \left\{\frac{\gamma_1}{(1+\gamma_1)}\left[\frac{W_0}{\lambda} - \lambda\left(\frac{1}{6} + \frac{1+\beta_1\Theta_0}{3(1+\beta_1)}\right)\right] + \frac{\lambda(2+\beta_1+\beta_1\Theta_0)}{2(1+\beta_1)}\right\}(g'^3\kappa\nu z)^{1/4}, \tag{6.19}$$

$$Nu_z = \frac{\beta_1(1-\Theta_0)}{(1+\beta_1)\lambda}\left(\frac{g'z^3}{\kappa\nu}\right)^{1/4}, \tag{6.20}$$

where, from (6.4) and (6.5), W_0 and Θ_0 satisfy

$$\frac{5}{3}\frac{E_1 W_0^2}{Pr^{1/2}} = \frac{4}{3}Pr^{1/2}E_1\Theta_0 - \frac{\gamma_1}{(1+\gamma_1)}\left[\frac{W_0}{\lambda} - \lambda\left(\frac{1}{6} + \frac{1+\beta_1\Theta_0}{3(1+\beta_1)}\right)\right], \tag{6.21}$$

$$E_1 W_0 \Theta_0 = \frac{\beta_1}{(1+\beta_1)\lambda Pr^{1/2}}(1-\Theta_0). \tag{6.22}$$

The value of λ is rather arbitrary and has no significance for laminar flow. When the flow is turbulent we estimate δ, the thickness of the laminar sublayer, by the position at which the eddy heat flux is one-tenth of the heat flux conducted down the mean temperature gradient and δ_i by the position at which the eddy and conducted fluxes are of the same magnitude (see figure 3 below.) In our model, λ is then given by the ratio δ/δ_i, as can be seen by comparing (3.15) with (6.10). In § 6.2 we find that this gives $\lambda = 0.4$ for turbulent flow. We use this value to determine numerical values of E_1, β_1 and γ_1 by comparing the power law solution to full analytic similarity solutions in two cases.

6.1.1. *Large-Prandtl-number expansions*

Kuiken (1968) derived the following asymptotic forms for the entrainment velocity, wall shear and local Nusselt number for large Pr:

$$v_e = \left(\frac{g'\kappa\nu}{4z}\right)^{1/4} 3[0.43 + 0.02Pr^{-1/2} + 0.07Pr^{-1} + O(Pr^{-3/2})], \tag{6.23}$$

$$\frac{\tau_w}{\rho_\infty} = (4g'^3\kappa\nu z)^{1/4}[0.82 - 0.31Pr^{-1/2} + 0.22Pr^{-1} + O(Pr^{-3/2})], \tag{6.24}$$

$$Nu_z = Ra_z^{1/4}[0.50 - 0.13Pr^{-1/2} + 0.05Pr^{-1} + O(Pr^{-3/2})]. \tag{6.25}$$

These truncated expansions show good agreement with full numerical solutions, with errors of less than 2% for Pr as small as 2 (Kuiken 1968). Comparison of these asymptotic expansions with our model predictions (6.18)–(6.20) generates the expansions

$$E_1 = 0.58 + 0.47Pr^{-1/2} + 0.08Pr^{-1} + O(Pr^{-3/2}), \tag{6.26}$$

$$\beta_1 = 0.25 + 0.09Pr^{-1/2} + 0.03Pr^{-1} + O(Pr^{-3/2}), \tag{6.27}$$

$$\gamma_1 = 0.53 - 0.44Pr^{-1/2} + 0.13Pr^{-1} + O(Pr^{-3/2}), \tag{6.28}$$

where we have set $\lambda = 0.4$ (as given in § 6.2.)

6.1.2. *Air with* $Pr = 0.71$

In order to compare with experimental data of Tsuji & Nagano (1988*a*), we will also need parameter values for air with $Pr = 0.71$. The correlations measured by Tsuji

& Nagano (1988*a*) for laminar flow are

$$Nu_z = 0.39 Ra_z^{1/4}, \tag{6.29}$$

$$\frac{\tau_w}{\rho} = 0.95 \left(\frac{Ra_z}{Pr} \right)^{1/12} (g'\nu)^{2/3}, \tag{6.30}$$

which are in excellent agreement with values obtained from a laminar similarity solution with $Pr = 0.71$ (see Gebhart *et al.* 1988, for example.) The laminar similarity solution also gives

$$v_e = 3Pr^{1/4} \left(\frac{g'\kappa\nu}{4z} \right)^{1/4} \times 0.60. \tag{6.31}$$

Matching (6.29)–(6.31) to the laminar power law solution (6.18)–(6.20) yields

$$E_1 = 3.1, \quad \beta_1 = 0.34, \quad \gamma_1 = 2.0. \tag{6.32}$$

The values of these parameters, determined from the analytic expressions for laminar flow, are used throughout the model, including when the flow is turbulent.

6.2. *Matching of model with experiment*

The values of E_2, β_2, γ_2, λ and Ra_c are estimated by comparison with the experimental measurements of Tsuji & Nagano (1988 *b*). They used a hot-wire technique to conduct detailed measurements of velocity, temperature and turbulent fluctuation profiles for a boundary layer in air, with $Pr = 0.71$. This lies in the regime $Pr = O(1)$; viscous and thermal length scales are comparable, and so we might expect that the general properties of the model for $Pr \geqslant O(1)$ should still apply.

We first estimate δ and δ_i by looking at the balance of conductive and turbulent heat fluxes provided by the experimental measurements. Typical near-wall profiles are shown in figure 3. We estimate δ_i to be the distance from the wall where the turbulent heat flux and mean conductive heat flux components are equal, i.e.

$$-\kappa \frac{\partial T}{\partial y}\bigg|_{y=\delta_i} = \overline{v'T'}|_{y=\delta_i}. \tag{6.33}$$

Similarly, we estimate δ using the distance where the turbulent heat flux exceeds a fraction $\epsilon = 0.1$ of the mean conductive heat flux,

$$-\epsilon\kappa \frac{\partial T}{\partial y}\bigg|_{y=\delta} = \overline{v'T'}|_{y=\delta}. \tag{6.34}$$

The choice $\epsilon = 0.1$ is somewhat arbitrary, as the inner-layer solution is derived for the limit $\epsilon \to 0$. For small values ($0.01 < \epsilon < 0.2$) the changes in predicted heat flux and wall shear are relatively small under variation of ϵ (changes of $<4\,\%$ and $<16\,\%$ over the entire integration range, respectively). For $\epsilon = 0.5$ the errors become larger (changes of $<9\,\%$ for heat flux and $<25\,\%$ for wall shear), perhaps reflecting the fact that the theory assumes $\epsilon \ll 1$. The values of δ and δ_i can be obtained from the intersections of the curves shown in figure 3. These values are used to calculate Ra_δ and Ra_{δ_i} as given in table 2. We then find values of b, W and T_o at four different heights by using the profiles of w and T measured by Tsuji & Nagano (1988 *b*) to approximate the numerical values of the integrals (4.16)–(4.18). The results are presented in table 2.

We can use the measured value of δ_i to predict a critical value of the global Rayleigh number Ra_z for transition between laminar and turbulent behaviour. We

Ra_z	$\hat{b}$	$\hat{W}$	Θ	Ra_δ	Ra_{δ_i}	$\lambda = \delta/\delta_i$
1.10×10^{10}	176	10.5	0.145	11.0	178	0.40
2.57×10^{10}	232	11.7	0.128	9.2	171	0.38
5.99×10^{10}	321	12.6	0.118	13.4	234	0.39
1.28×10^{11}	357	14.7	0.109	9.8	139	0.41

TABLE 2. Estimates of $\hat{b} = b(g'\kappa)^{1/3}/\nu$, $\hat{W} = W/(g'\kappa)^{1/3}$, $\Theta = (T_o - T_\infty)/(T_w - T_\infty)$, Ra_δ, Ra_{δ_i}, and λ at four values of Ra_z using the experimental data of Tsuji & Nagano (1988*b*). The values of $\hat{b}$, $\hat{W}$ and Θ are compared to the prediction of the model in Figure 6. The values of Ra_δ and Ra_{δ_i} are each of approximately constant size, consistent with the prediction (3.28).

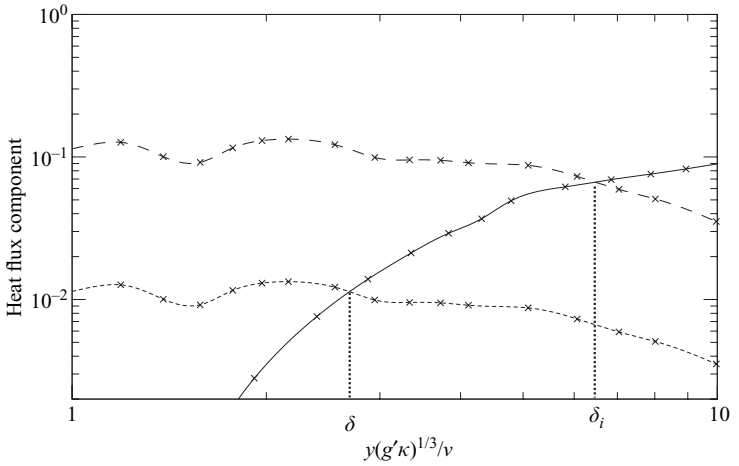

FIGURE 3. Plot of near-wall heat flux component variations, using hot-wire measurement data from the experiments of Tsuji & Nagano (1988*b*). Measurements of the conductive heat flux $-\kappa T_y$ are joined by a long-dashed line and measurements of the turbulent heat flux $\overline{v'T'}$ are joined by a solid line. The short-dashed line represents $-0.1\kappa T_y$. All heat flux components are non-dimensionalized by $(g'\kappa)^{1/3}(T_w - T_\infty)$. The long-dashed and solid curves intersect at the length scale δ_i according to the criterion (6.33), so that conducted and turbulent fluxes are equal at this point. The length scale δ is given by the intersection of the short-dashed and solid curves, when the turbulent flux exceeds a critical fraction of the conducted flux as given by (6.34).

recall from (3.15) that the inner length scale for laminar flow satisfies $\delta_i \sim z Ra_z^{-1/4}$ and increases with height z, while (3.28) implies that δ_i is initially constant for turbulent flow. We enforce the transition from laminar to turbulent flow models when these two scales for δ_i coincide. The values in table 2 suggest that $Ra_{\delta_i} \approx 180$ for turbulent flow. We can therefore predict the transition from laminar to turbulent behaviour when

$$Ra_z = Ra_{\delta_i}^4 \equiv Ra_t, \tag{6.35}$$

where the constant

$$Ra_t = 180^4 \approx 10^9. \tag{6.36}$$

We will see in § 6.3 that this prediction is a good approximation to the observed change from laminar behaviour in the experiments of Tsuji & Nagano (1988*a*), and it is also consistent with other experimental studies (see Schlichting 1968, p. 303).

We also note that the ratio $\lambda = \delta/\delta_i$ is approximately constant, so that asserting $\delta \propto \delta_i$ appears to be a decent approximation. We set

$$\lambda = 0.4, \tag{6.37}$$

so that

$$Ra_c = \lambda^3 Ra_{\delta_i} = 11. \tag{6.38}$$

The entrainment constant E_2 is estimated by substituting measured values of v and W into the entrainment law

$$v(\infty) = -E_2 W. \tag{6.39}$$

Measurements of v were available only for $Ra_z = 6.36 \times 10^{10}$, and so we take the value of v at the boundary layer edge as an estimate for the entrainment velocity $v(\infty)$, yielding an entrainment coefficient

$$E_2 = 0.135. \tag{6.40}$$

This is of a similar order of magnitude to the value $E \approx 0.1$ found by Wells & Wettlaufer (2005) for density currents flowing down a vertical wall, and is also consistent with an extrapolation of the data of Ellison & Turner (1959) to vertical flows.

The values of β_2 and γ_2 were fixed by comparing the predicted heat flux q_w and wall shear τ_w, based on measured W and T_o values, to the observed values of q_w and τ_w at the single point $Ra_z = 1.28 \times 10^{11}$ where the turbulent flow is most developed. Tsuji & Nagano (1988*a*) observe

$$Nu_z = 605, \qquad \tau_w/\rho(g'\nu)^{1/3} = 6.04, \qquad \text{at} \quad Ra_z = 1.28 \times 10^{11}. \tag{6.41}$$

We then use (6.1)–(6.9) to give expressions for the predicted values of Nu_z and τ_w in terms of β_1, γ_1, E_2, W, T_o, Ra_c, β_2 and γ_2. The parameters β_1, γ_1, E_2, W, T_o, and Ra_c are all known, and so matching predicted and observed values of q_w and τ_w gives two conditions for β_2 and γ_2, yielding

$$\beta_2 = 0.023, \quad \gamma_2 = 0.063. \tag{6.42}$$

The final condition is to select a value of Re_c. There are no experimental data in the shear instability regime, and so we compare to the critical Reynolds number for instability of a Blasius boundary layer generated by forced flow past a flat plate. The critical Reynolds number based on momentum thickness given by Schlichting (1968) is $Re_{\delta_1} = 420$. We expect instability when $Re_{\delta_i} \sim Re_{\delta_1}$, and so we use the critical value

$$Re_\delta = Re_c = 420\lambda. \tag{6.43}$$

for comparison with Tsuji & Nagano (1988*a*, *b*) experimental data in air with $Pr < 1$. Note however that the value of Re_c might have some Prandtl number dependence for $Pr \gg 1$ as can be seen by considering the scaling condition (3.29). The final parameter values used are summarized in table 3.

6.3. *Numerical integration for turbulent flow*

With the parameter values in table 3, we integrated equations (6.3)–(6.14) numerically using the Maple routine '`dsolve rkf45`'. The equations were integrated from $Ra_z = 5 \times 10^{-10}$ with initial conditions $b(g'\kappa)^{1/3}/\nu = 0.735$, $W/(g'\kappa)^{1/3} = 0.012$ and $(T_o - T_\infty)/(T_w - T_\infty) = 0.394$ given by the laminar power law solution (6.15)–(6.17). The numerical simulations show near-exact agreement with the power law solution in the laminar regime. We switch to the buoyant instability regime when $Ra_z = Ra_t$.

Parameter	λ	$Ra_t = Ra_{\delta_i}^4$	Ra_c	Re_c	E_1	β_1	γ_1	E_2	β_2	γ_2
Value	0.4	10^9	11	420λ	3.1	0.34	2.0	0.135	0.023	0.063
Source	(1)	(1)	$Ra_c = \lambda^3 Ra_{\delta_i}$	(3)	(2)	(2)	(2)	(1)	(1)	(1)

TABLE 3. Summary of parameter values used in numerical calculations for $Pr = 0.71$. (1) Estimate from the data of Tsuji & Nagano (1988*b*). (2) Laminar similarity solution. (3) Blasius boundary layer instability (Schlichting 1968). Note that these values have been obtained from experimental results for air – it is possible they may have some Prandtl number dependence.

We generically find that W grows in the buoyant instability regime, so that the shear instability criterion is always activated at large z. We emphasize that the choice of parameters shown in table 3 only changes the length over which each regime runs and the magnitude of each of the variables: it does not affect the functional form of the z-dependence.

Figure 4 shows typical plots of Nusselt number and non-dimensional wall shear, with the laminar scaling observed for $Ra_z < 10^9$, the turbulent buoyant instability solution for $10^9 < Ra_z < 1.2 \times 10^{16}$ and a transition to the shear instability regime for $Ra_z > 1.2 \times 10^{16}$.

Figure 4(*b*) also shows the variation of τ and the outer buoyancy force $gb\alpha(T_o - T_\infty)$. In the buoyant instability regime, τ_w is significantly larger than τ, so that $g'\delta \gg \tau$ and the buoyancy contribution from the inner conductive sublayer is important, consistent with the ideas presented in the scaling analysis. Also, we see that τ approaches τ_w as we enter the shear instability regime, consistent with the idea that the shear exerted at $y = \delta$ dominates the sublayer buoyancy force in this limit, so that $\tau \gg g'\delta$.

In order to examine more closely the transition between laminar and turbulent behaviour, figure 5 shows the variation of Nu with Ra_z on linear scales close to the transition point. We recall that we have used measurements of the local turbulent fluctuation profiles over the range $10^{10} < Ra_z < 10^{11}$ in order to estimate δ_i and hence predict $Ra_t = Ra_{\delta_i}^4 = 10^9$ according to (6.35). This prediction of Ra_t compares favourably with the deviation between laminar and turbulent behaviour of the Nusselt number observed in the experiment. The computed value of Nu compares well with the measured value, with all errors smaller than 18 %. This agreement is encouraging, especially given that the prediction is made without any fitting parameters.

The z-variations of b, W and T_o are shown for laminar and buoyant instability regimes in figure 6. The velocity W matches the experimental measurements well. The outer-layer width b and temperature T_o show less satisfactory quantitative agreement, but still capture the qualitative pattern of z-dependence. The disagreement in temperature and plume width values might be explained by the observed presence of an ambient temperature stratification in the experiments of Tsuji & Nagano (1988*a*), which would alter the balance in the heat equation. The error in prediction of plume width is also consistent with using too large an entrainment constant. The value $E = 0.135$ is based on only one set of boundary layer profiles and is slightly larger than previous estimates (e.g. Wells & Wettlaufer 2005 give $E = 0.1$). There is also likely to be significant error involved in numerically approximating the integrals (4.16)–(4.18) which extend over an infinite domain, and the assumption of self-similarity of the profiles of the outer flow could also be another source of error. The numerical solution approaches limits for each of the buoyant and shear instability regimes, which are derived below.

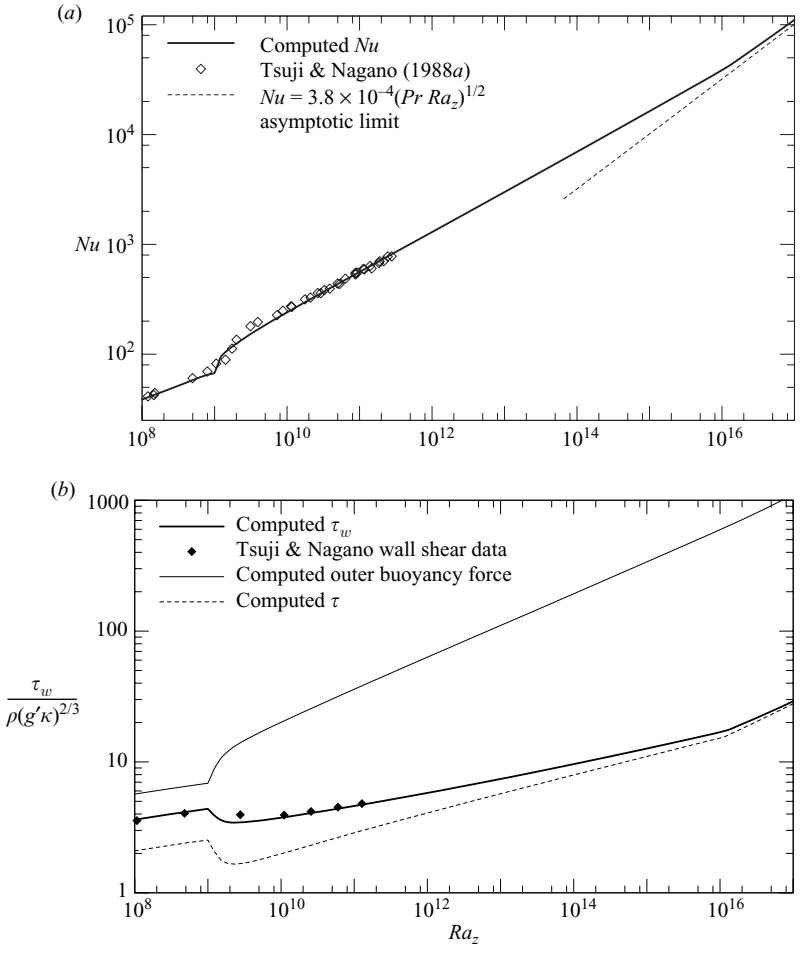

FIGURE 4. Numerical simulation of integrated profiles for the outer turbulent flow, plotted against Ra_z on log scales. (*a*) Comparison of calculated Nusselt number to experimental measurements, and shear instability large z asymptotic limit. (*b*) Comparison of calculated non-dimensional wall shear $\tau_w/\rho(g'\kappa)^{2/3}$ to experimental observation, calculated outer buoyancy force and calculated shear coupling between layers. Experimental data taken from Tsuji & Nagano (1988*a*, *b*).

6.4. *The constant heat flux limit with a buoyancy-driven sublayer*

For moderate z, figure 4(*b*) shows that the shear coupling τ is significantly smaller than the shear exerted at the wall τ_w, implying that buoyancy is dominant in driving the conductive sublayer. In addition, τ is much smaller than the outer buoyancy, and so we can neglect τ from the outer momentum balance (6.4). We also have $T_o - T_\infty \ll T(\delta) - T_\infty$, and $\beta_2 E_2 W\delta/\kappa \ll \beta_1$. Hence q is approximately constant at leading order in (6.8), implying q_w is constant, consistent with the experimental correlation

$$Nu = 0.120 Ra_z^{1/3} \tag{6.44}$$

observed by Tsuji & Nagano (1988*a*).

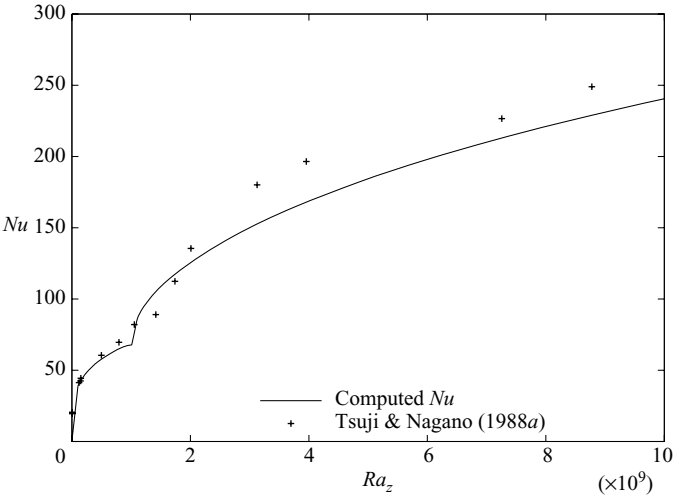

FIGURE 5. Comparison of calculated Nusselt number to experimental measurements, both plotted as a function of Ra_z on linear scales close to the transition point between laminar and turbulent behaviour. Experimental data taken from Tsuji & Nagano (1988a, b).

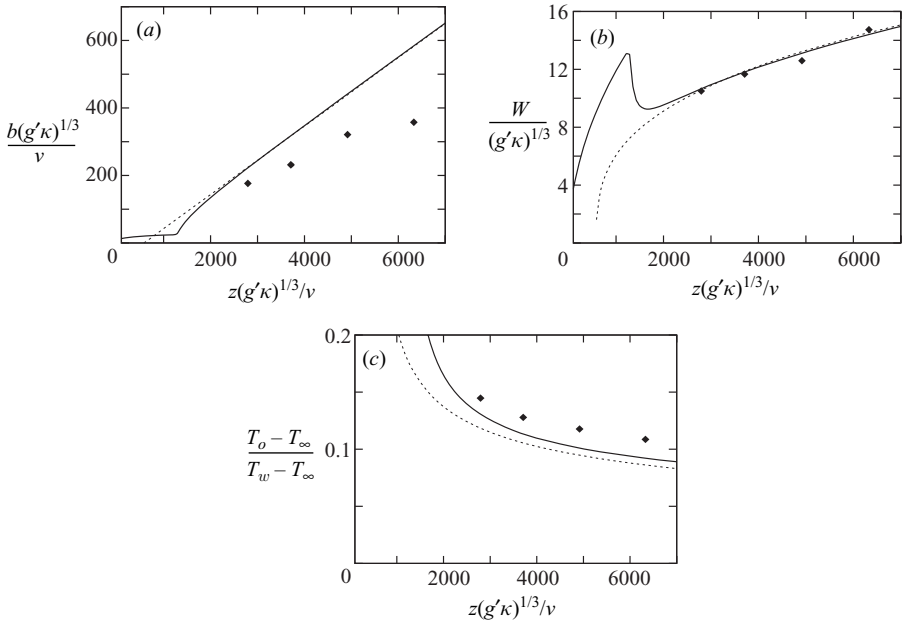

FIGURE 6. Plots of (a) outer plume width $b(g'\kappa)^{1/3}/\nu$, (b) velocity $W/(g'\kappa)^{1/3}$ and (c) temperature $(T_o - T_\infty)/(T_w - T_\infty)$. The numerical solution (solid curves) is compared with values estimated from the experimental data of Tsuji & Nagano (1988 b) (symbols) and the buoyant instability asymptotic limit (dashed curves.) The transition from laminar to turbulent flow occurs at $z(g'\kappa)^{1/3}/\nu = 1260$.

Hence, we can approximate the dimensional governing equations (6.3)–(6.5) by

$$\frac{\mathrm{d}}{\mathrm{d}z}(bW) = E_2 W, \tag{6.45}$$

$$\frac{\mathrm{d}}{\mathrm{d}z}(bW^2) = bg\alpha(T_o - T_\infty), \tag{6.46}$$

$$\frac{\mathrm{d}}{\mathrm{d}z}\left[bW\,(T_o - T_\infty)\right] = \frac{\beta_1}{(1+\beta_1)(Pr\,Ra_c)^{1/3}}(g'\kappa)^{1/3}(T_w - T_\infty), \tag{6.47}$$

at leading order. This system has a power law solution

$$b = \frac{3}{4}E_2 z, \tag{6.48}$$

$$W = \left[\frac{4\beta_1}{5E_2(1+\beta_1)(Pr\,Ra_c)^{1/3}}\right]^{1/3}(g'\kappa)^{1/9}(g'z)^{1/3}, \tag{6.49}$$

$$T_o - T_\infty = \frac{5}{3\,Pr}\left[\frac{4\beta_1\,Pr}{5E_2(1+\beta_1)(Pr\,Ra_c)^{1/3}}\right]^{2/3}(T_w - T_\infty)\left[\frac{\nu}{(g'\kappa)^{1/3}\,z}\right]^{1/3}. \tag{6.50}$$

Figure 6 compares the numerical and experimental results to these asymptotic limits (6.48)–(6.50), after a virtual origin correction

$$z \to z - 700\nu/(g'\kappa)^{1/3} \tag{6.51}$$

is made visually, to allow for the effects of starting the turbulent regime with non-zero mass, momentum and buoyancy fluxes (such corrections are often required in plume calculations, e.g. Linden 2000). The velocity and boundary layer width show good agreement with the numerical solution, and the temperature shows a reasonable qualitative fit. The solution above breaks down as W increases and significantly alters the value of β in the heat balance, subsequently affecting the temperature. This effect explains the larger discrepancy between the analytic limit and the numerical temperature solutions.

As W increases, τ eventually becomes comparable to the $O(g'\delta)$ inner buoyant forcing. The shear instability criterion (6.13) is met at $Ra_z = 1.2 \times 10^{16}$ and a new flow regime develops. This would correspond to a height of 140 m in the Tsuji & Nagano (1988*a*) experiments in air – beyond the scope of laboratory experiment but of probable importance in a geophysical context.

6.5. *The shear-driven sublayer limit*

The moderate z-solution discussed above has constant inner buoyancy, while the outer buoyancy continually grows due to the constant heat flux to the outer layer. Hence the outer velocity W will grow and exert an increasing upward shear on the conductive sublayer. Eventually W becomes sufficiently large that the inner layer width is controlled by the shear instability criterion (6.13). In this limit, the inner flow is effectively passive, acting only to provide a drag opposing the outer flow. We obtain a large-z asymptotic limit

$$\frac{\tau}{\rho_\infty} = K_f W\,|W|\,, \tag{6.52}$$

$$\frac{q}{\rho_\infty c_p} = St\,|W|\,(T_w - T_o), \tag{6.53}$$

where we identify

$$K_f = \frac{\gamma}{(1+\gamma)Re_c} = 0.0046 \tag{6.54}$$

as the drag coefficient, and

$$St = \frac{\beta}{(1+\beta)PrRe_c} = 0.0035 \tag{6.55}$$

as the Stanton number. We have used the notation

$$\beta = \beta_1 + \beta_2 E_2 PrRe_c, \quad \gamma = \gamma_1 + \gamma_2 E_2 Re_c, \tag{6.56}$$

here. These forms of scaling law are commonly used for forced convection in engineering applications (see Incropera & De Witt 2002, for example.) We can think of the outer buoyancy generating an outer flow strong enough for a forced convective flow to develop in the inner conductive sublayer. The quadratic drag law (6.52) is also commonly used for geophysical-scale models of wall-bounded density currents (see Hughes & Griffiths 2006, for example) and has been applied to model the basal drag of tidal currents by Taylor (1920). These typically use a drag coefficient $K_f = O(10^{-3})$, giving good order of magnitude agreement with (6.54). McPhee *et al.* (1999) measured a Stanton number for turbulent forced flow under sea ice, and found $0.005 < St < 0.006$, which again gives good order of magnitude agreement with our estimated value. It is encouraging to note that our predictions of K_f and St, based on laboratory-scale measurements of the turbulent flow properties, are consistent with estimates from geophysical-scale data for forced flow.

Using (6.52) and (6.53), we obtain dimensional governing equations

$$\frac{\mathrm{d}}{\mathrm{d}z}[bW] = EW, \tag{6.57}$$

$$\frac{\mathrm{d}}{\mathrm{d}z}[bW^2] = \alpha g b(T_o - T_\infty) - K_f W|W|, \tag{6.58}$$

$$\frac{\mathrm{d}}{\mathrm{d}z}[bW(T_o - T_\infty)] = St|W|(T_w - T_o), \tag{6.59}$$

which admit a power law solution

$$b = \frac{2E}{3}z, \tag{6.60}$$

$$W = \left[\frac{2E\,St}{(4E+3K_f)(St+E)}\right]^{1/2}(g'z)^{1/2}, \tag{6.61}$$

$$T_o - T_\infty = \frac{St}{St+E}(T_w - T_\infty), \tag{6.62}$$

$$\frac{q}{\rho_\infty c_p} = \left[\frac{2E^3\,St^3}{(4E+3K_f)(St+E)^3}\right]^{1/2}(g'z)^{1/2}. \tag{6.63}$$

The last of these conditions implies that

$$Nu_z = A(PrRa_z)^{1/2}, \tag{6.64}$$

where the constant A takes the value

$$A = 3.8 \times 10^{-4} \tag{6.65}$$

for the parameter values relevant to the Tsuji & Nagano (1988*a*) experiments in air. The analysis presented does not preclude the possibility that the constant A depends on the Prandtl number Pr. However, if the entrainment coefficient E and the bulk transfer coefficients St and K_f are all independent of Pr, then A is also independent

of Pr and the result (6.64) is interestingly independent of viscosity. Figure 4 shows the numerically calculated Nu approaching the limit (6.64) for large Ra_z. Note that this correlation is valid only when the shear instability criterion (6.13) has been met, for

$$Ra_z > 1.2 \times 10^{16} \tag{6.66}$$

in the case of air. Hence, this correlation is beyond the scope of previous laboratory experiments, but may be of importance on geophysical scales. The threshold value and the constant A may have some dependence on Prandtl number, but we are unable to determine the form of this dependence without further experimental data.

7. Conclusions

We have used scaling to show that a turbulent natural convection boundary layer can be considered as comprising three distinct sublayers, with a near-wall laminar conductive region, an intermediate viscous–turbulent layer and an outer inertial–turbulent region. Two possible turbulent flow regimes are found, depending on the force balance in the inner region of the flow. If the inner region is driven by its own buoyancy we predict a constant wall heat flux, which recovers the scaling $Nu_z \propto Ra_z^{1/3}$ previously observed in laboratory experiments. At larger scales, the buoyancy in the outer part of the flow generates a strong outer velocity, which then exerts a shear to drive the inner section of the flow. The dynamics of the flow is then well described by plume-like equations for the outer velocity, incorporating heat transfer and drag laws similar to those used for forced convection. This predicts the correlation $Nu_z \propto Ra_z^{1/2}$, which gives rise to significantly larger predictions of heat transfer on geophysical scales.

A unified model has been developed (see table 1) that can be used to determine the evolution of the heat flux and wall shear with height, varying from a laminar state through two different turbulent states. The constant parameters have been determined for air (table 3) by comparison with an analytic solution of the laminar regime and by fitting to data at a fixed height in the first turbulent regime. We might, however, expect these parameters to have some Prandtl number dependence, so that the values may differ slightly for water. The model is shown to make predictions in good agreement with the observed variations of heat flux and wall shear in the laminar and first turbulent regime. It also predicts a heat transfer coefficient (Stanton number) and drag coefficient in the second turbulent regime which are in good agreement with geophysical measurements of forced convection in water. This suggests that any Prandtl number dependence may be relatively weak.

The transitions between the flow regimes are consistent with a hierarchy of instabilities for the laminar sublayer. The flow is initially laminar before a criterion consistent with a buoyant instability is attained, and turbulent fluctuations are generated. This criterion accurately predicts the observed height of transition between laminar and turbulent behaviour of the heat flux. The final turbulent regime is predicted to occur when the Reynolds number exceeds a critical value consistent with a shear instability dominating the inner flow. We find a corresponding variation in the width of the laminar sublayer, which increases with height for laminar flow, is constant in the buoyant instability regime and then decreases as height increases in the shear instability regime.

The predicted variation in heat flux has important consequences for the melting rate of vertical ice surfaces. For example, the melt rate of a polar ice shelf must satisfy the Stefan condition, giving a melt rate proportional to heat flux. The melt

rate decreases with height in the laminar regime, then attains a constant value in the turbulent buoyant instability regime. Finally, on geophysical scales, we expect the melt rate to increase with height when the shear-instability regime is attained. This second turbulent regime is particularly relevant for consideration of solutal convection next to ice in sea water, where the relevant Rayleigh numbers are typically larger owing to the stronger solutal buoyancy and smaller solutal diffusivity D (for example, $g'z^3/D\nu \approx 10^{20}$ for an ice surface submerged 100 m into sea water of salinity 35 psu.) The correlation $Nu_z \propto Ra_z^{1/2}$ in (6.64) then predicts a wall salt flux 10 times larger than would be given using the correlation $Nu_z \propto Ra_z^{1/3}$ in (6.44). This difference in salt transfer would have a significant influence on more complex models of ice ablation, which may also need to account for the effects of two-component convection, stratification, ambient currents and a non-planar ice interface. The ideas presented here therefore require further experimental investigation at larger Ra_z to confirm or discount the correlation $Nu_z \propto Ra_z^{1/2}$, and its relevance to geophysical flows.

We are grateful to Herbert Huppert for helpful comments on an earlier draft of this work. This research was partially supported by a NERC PhD studentship to A. J. W., award NER/S/A/2005/13260.

REFERENCES

Ellison, T. H. & Turner, J. S. 1959 Turbulent entrainment in stratified flows. *J. Fluid Mech.* **6**, 423–448.

Gebhart, B., Jaluria, Y., Mahajan, R. L. & Sammakia, B. 1988 *Buoyancy Induced Flows and Transport*, chap. 11, pp. 547–655. Hemisphere.

George, W. K. & Capp, S. P. 1979 A theory for natural convection turbulent boundary layers next to heated vertical surfaces. *Intl J. Heat Mass Transfer* **22**, 813–826.

Hieber, C. A. & Gebhart, B. 1971 Stability of vertical natural convection boundary layers: Expansions at large Prandtl number. *J. Fluid Mech.* **49**, 577–591.

Hölling, M. & Herwig, H. 2005 Asymptotic analysis of the near-wall region of turbulent natural convection flows. *J. Fluid Mech.* **541**, 383–397.

Hughes, G. O. & Griffiths, R. W. 2006 A simple convective model of the global overturning circulation, including effects of entrainment into sinking regions. *Ocean Modell.* **12**, 46–79.

Incropera, F. P. & De Witt, D. P. 2002 *Fundamentals of Heat and Mass Transfer*, 5th edn. Wiley.

Josberger, E. G. & Martin, S. 1981 A laboratory and theoretical study of the boundary layer adjacent to a vertical melting ice wall in salt water. *J. Fluid Mech.* **111**, 439–473.

Kuiken, H. K. 1968 An asymptotic solution for large Prandtl number free convection. *J. Engng Maths* **2**, 355–371.

Kutateladze, S. S., Kirdyashkin, A. G. & Ivakin, V. P. 1972 Turbulent natural convection on a vertical plate and in a vertical layer. *Intl J. Heat Mass Transfer* **15**, 193–202.

Linden, P. F. 2000 *Perspectives in Fluid Mechanics*, chapter 6: Convection in the environment, pp. 303–321. Cambridge University Press.

McPhee, M. G., Kottmeier, C. & Morison, J. H. 1999 Ocean heat flux in the Central Weddell Sea during winter. *J. Phys. Oceanogr.* **29**, 1166–1179.

Morton, B. R., Taylor, G. & Turner, J. S. 1956 Turbulent gravitational convection from maintained and instantaneous sources. *Proc. R. Soc. Lond.* A **234**, 1–23.

Nachtsheim, P. R. 1963 Stability of free-convection boundary-layer flows. *Tech. Rep.* NASA TN D–2089.

Ostrach, S. 1952 An analysis of laminar free-convection flow and heat transfer about a flat plate parallel to the direction of the generating body force. *NACA-TN.* 2635.

Papailiou, D. D. 1991 Turbulence models for natural convection flows along a vertical heated plane. *Tech. Rep.* AGARD-A-R-291 4-1 to 4-5.

RUCKENSTEIN, E. 1998 On the laminar and turbulent free convection heat transfer from a vertical plate over the entire range of Prandtl numbers. *Intl Commun. Heat Mass Transfer* **25**, 1009–1018.

SCHLICHTING, H. 1968 *Boundary Layer Theory*, 6th edn., p. 452 McGraw-Hill.

TAYLOR, G. I. 1920 Tidal friction in the Irish Sea. *Philos. Trans. R. Soc. Lond.* A **220**, 1–33.

TSUJI, T. & NAGANO, Y. 1988*a* Characteristics of a turbulent natural convection boundary layer along a vertical flat plate. *Intl J. Heat Mass Transfer* **31**, 1723–1734. (Data taken from www.ercoftac.org.)

TSUJI, T. & NAGANO, Y. 1988*b* Turbulence measurements in a natural convection boundary layer along a vertical flat plate. *Intl J. Heat Mass Transfer* **31**, 2101–2111. (Data taken from www.ercoftac.org.)

WELLS, M. G. & WETTLAUFER, J. S. 2005 Two-dimensional density currents in a confined basin. *Geophys. Astrophys. Fluid Dyn.* **99**, 199–218.